Sputtering and Thermal Evaporation Studies of Lithiated ATJ Graphite

Kenzo Ibano, *Member, IEEE*, Vijay Surla, and David N. Ruzic, *Member, IEEE*

***Abstract*—Sputtering yields and thermal evaporation fluxes of lithium and lithiated ATJ graphite are studied. Sputtering yields are measured for the ATJ graphite by lithium ion bombardment at 45° incidence, with 700–2000 eV accelerations. Typically, 4×10^{13} ions/(cm$^2 \cdot$ s) flux of Li ion beam is obtained from LiCl powder in a Colutron ion source. Sputtered particles are collected by a quartz crystal microbalance to determine sputtering yields. The experiment is repeated after Li is evaporated onto the ATJ graphite target. Suppressed amounts of sputtered particles are observed after Li treatment. Deuterium (D) saturation treatment for lithiated graphite is also done to simulate actual divertor conditions. The sputtering yield after D saturation does not show distinct difference with nonsaturated samples. In addition, thermal evaporation fluxes of Li on stainless steel (SS) and intercalated Li in the ATJ graphite are measured. An interesting finding is that Li in graphite shows a magnitudeless evaporation flux than Li on SS for surface temperatures ranging from 250 °C to 500 °C.**

***Index Terms*—Divertor, graphite, lithium, sputtering.**

I. Introduction

LITHIUM evaporation treatments for ATJ graphite tiles of divertor regions in the National Spherical Torus Experiment have shown a number of dramatic improvements for its plasma performance: confinement time, low carbon impurity rate, low-hydrogen recycling, suppressing ELMs, and so on [1]. Previous laboratory studies [2] showed that evaporated Li intercalates into the graphite bulk region and might form a very thin layer (a few monolayers) on the surface. This low-Z Li layer is preferentially sputtered from the surface and prevents chemical reaction between hydrogen and graphite. Furthermore, it is predicted that, because of high diffusivity of Li in the graphite, Li atoms in the graphite bulk region segregate to the surface quickly, forming a new layer after the Li layer is sputtered off.

However, it is possible that the Li that is evaporated or sputtered off could be ionized and would come back to the wall with accelerations. Hence, this necessitates the experimental measurements of sputtering yields of Li^+ on graphite. In this paper, ATJ graphite samples are irradiated by Li^+ at 45° incidence, which is the average angle of incidence at the divertor region [3]. It is also important to know the sputtering yields of Li^+ on deuterium (D)-saturated and nonsaturated lithiated graphite because lithiated graphite tiles in an actual device could be saturated by D after a shot. Previous study [4] showed that D saturation for solid Li when sputtered by He^+ suppresses its sputtering yield as a result of the preferential sputtering of light D atoms. Therefore, Li-evaporated ATJ graphite (Li/C) and D-saturated ATJ graphite (D-Li/C) target samples are prepared, and their sputtering yields are examined.

Another important question for the lithiated graphite divertor is whether intercalated Li in graphite evaporates from the surface as bulk Li does or does not. The lithiated graphite divertor currently has a maximum temperature limit of around 400 °C because of the low melting temperature of bulk Li. If the intercalated Li in graphite has a lower evaporation flux than bulk Li, that temperature limit can be set higher than now. In order to answer this question, the evaporation flux of intercalated Li in graphite at different temperatures is measured and compared with the evaporation flux of the Li layer on stainless steel (SS).

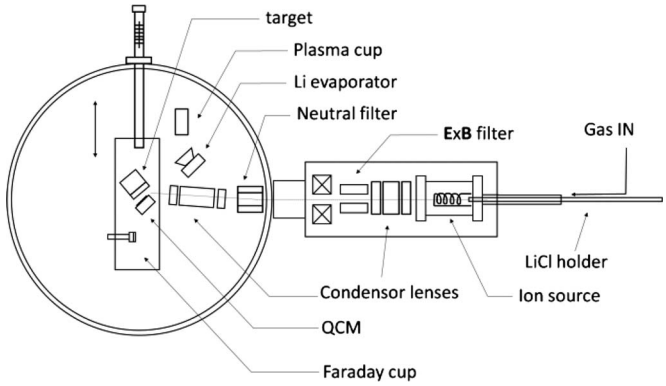

Fig. 1. Schematic of the experimental setup of IIAX. The left chamber is the main chamber where the QCM, the sputtering target, the lithium evaporator, and the plasma cup are located. The right chamber is the ion gun chamber where the Colutron ion source, the condenser lenses, and the $\mathbf{E} \times \mathbf{B}$ filter are located.

II. Experimental Setup

A. IIAX

In this paper, the Ion-surface InterAction eXperiment (IIAX) at University of Illinois at Urbana–Champaign is used to measure the sputtering yields of ATJ graphite. IIAX consists of two connected vacuum chambers: a 24-in-diameter cylindrical main chamber and an ion gun chamber with a Colutron ion source, as shown in Fig. 1. The base pressures are around 10^{-5} Pa. Li^+ beam is generated at the Colutron ion source using the LiCl powder. First, the LiCl powder is heated up and dissociated by

Manuscript received June 29, 2009; revised November 6, 2009. First published January 22, 2010; current version published March 10, 2010. This work was supported by DOE/ALPS under Contract DEFG02-99ER54515.

The authors are with the Department of Nuclear, Plasma, and Radiological Engineering, University of Illinois at Urbana–Champaign, Urbana, IL 61801 USA (e-mail: kibano@gmail.com; vijay.surla@gmail.com; druzic@illinois.edu).

Color versions of one or more of the figures in this paper are available online at http://ieeexplore.ieee.org.

Digital Object Identifier 10.1109/TPS.2009.2037907

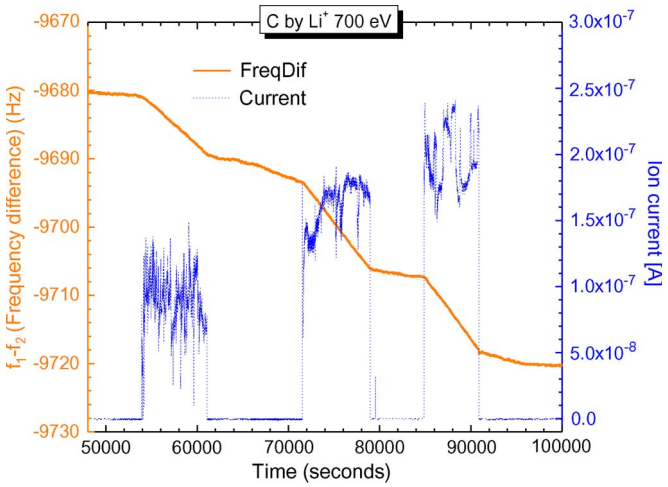

Fig. 2. Typical data of the sputtering measurement. The frequency changes of QCM and the ion current on the target are plotted together. The decreasing frequency corresponds to the increasing mass on the crystal.

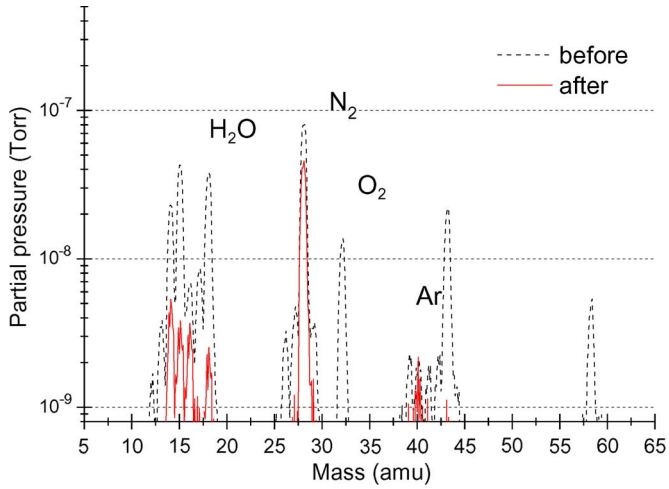

Fig. 3. Comparison of the partial pressures of the impurity gas in the chamber before and after the lithium gettering treatment.

Ar arc plasma. Then, the applied electric potential accelerates out Ar^+ and Li^+ ions from the ion chamber. After being focused by the first set of condenser lenses, these ions are separated at an $\mathbf{E} \times \mathbf{B}$ filter by their mass difference. By this filtering, only Li^+ and some neutrals reach the main chamber. The measured ion current at the main chamber as a function of the applied voltage of this filter is recorded to find the optimal voltage for producing the Li^+ beam. To obtain lighter ions, a higher electric field is required because the $\mathbf{v} \times \mathbf{B}$ force is larger for lighter ions. In the main chamber, neutral particles are eliminated by a neutral filter, and ions are focused again by second condenser lens. Finally, only the desired ions reach the ATJ graphite target that has a 1-mm thickness and an area of 507 mm^2. Before irradiating these targets, the ion current is measured using a 2-mm-diameter Faraday cup with a pi-coammeter. Typical current measured is around 200 nA, which corresponds to a flux of 4×10^{13} ions$/(\mathrm{cm}^2 \cdot \mathrm{s})$. The Faraday cup and a sample holder are held on a single sliding stage so that the target is set in front of the beam by sliding the stage after current measurement through the Faraday cup. During sample irradiation, current on the sample is also measured and recorded.

For the evaporation measurements, a ultrahigh vacuum (UHV) heater behind the sample is heated by a controlled ac power supply. A type-K thermocouple is attached to the heater in order to have a precise temperature control. Calibration measurements are taken to find the corresponding surface temperatures with the heater temperature.

Sputtered or evaporated material from the target is collected by a quartz crystal microbalance (QCM). QCM measures its mechanical vibration frequency by a resonance method. The mass deposition rate on crystal can be calculated through frequency changes. The QCM system in IIAX employs dual crystals, where one crystal measures the frequency change from the sputtering material, while the other measures only the background signal. Typical data obtained from the QCM are shown in Fig. 2. When the beam is on, the QCM frequency drops, which corresponds to the increasing mass on the crystal. The frequency change when the beam is off is considered as the background signal came from the oxidation of lithium on the QCM surface and subtracted from the frequency change when the beam is on.

B. Lithium Deposition and D Saturation

Li is deposited using an *in situ* Li evaporator. First, a piece of solid Li ribbon is placed inside the cup of the evaporator in an Ar ambient to avoid contaminations of Li by oxygen and nitrogen impurities. After the main chamber was pumped out, a UHV heater below the cup is heated to 500 °C. Keeping the shutter of the Li evaporator closed, Li gettering is performed to reduce impurities of the chamber. During this gettering process, partial pressures of the impurity gas in the chamber are measured by a quadrupole residual gas analyzer (RGA). Comparing before and after Li gettering, a significant reduction of water and oxygen impurities is seen, as shown in Fig. 3. However, because of the zero-blast problem of the quadrupole RGA, reduction of hydrogen impurities cannot be examined.

Li is evaporated on graphite for about 10 min with a flux of 1×10^{18} atoms$/(\mathrm{cm}^2 \cdot \mathrm{s})$ from the source. This high-temperature fast evaporation was chosen to avoid the contamination of Li from the oxidation. It is predicted that the fraction of the evaporated material was mainly Li since the fluxes of residual impurities were negligible compared with the Li flux. The amount of evaporated Li to graphite is usually denoted by an equivalent thickness because no distinct layer would appear on the graphite surface. This equivalent thickness is estimated by the known vapor pressure of Li and the distance between the heater and the target. In this estimation, the Li flux was calculated from the known vapor pressure, and the fraction reaching to the target was assumed as $Area/\pi d^2$, where d is the distance between the heater and the target. Since the deposition rate is sensitive to this distance, the sample holder is set carefully at the same position for each deposition treatment by using a measure of the *in vacuo* motion feedthrough. In addition, the estimated thickness is calibrated by measuring the Li layer thickness on a masked witness Si plate just below the sample by a profilometer. Although this witness plate method does not answer how far lithium diffuses into the graphite bulk region,

it is useful to know how much amount of lithium is deposited to the graphite surface. The typical thickness evaporated to the sample is around 1 ± 0.2 μm. The uncertainty came from the oxidation effect of the lithium layer.

For the D saturation of Li, a plasma cup is used, which is a simple combination of cylindrical anode and cathode with a dielectric barrier between them. After filling the chamber with 15 Pa of D_2, a voltage of 400 V is applied between the electrodes to ignite the dc discharge, which is then used to irradiate the sample. Typical flux in the order of 10^{15} ions/(cm$^2 \cdot$ s) is obtained. The flux is calculated from the measured ion current by an ammeter.

C. Sputtering Yield Calculation

Sputtering yield is defined as the average number of atoms ejected from the surface per incident ion. It can be calculated from the mass change on the QCM crystal and measured ion dose as

$$Y_o = \frac{1}{m_* S I_{\text{ion}} f_{\text{geo}}} \frac{\partial m}{\partial t}$$

where m_* is the atomic mass of the sputtered material; S is the sticking coefficient of the sputtered material to the QCM crystal, which is estimated by the computer calculations; I_{ion} is the ion dose on the sample; f_{geo} is the calculated fraction of the sputtered material reaching the QCM crystal with an assumption of the cosine distribution; and $\partial m/\partial t$ is the mass change on the QCM crystal. Special care is taken in determining I_{ion} because π electrons of graphite are easily released by collisions and its removal from the surface increases the net positive current. Therefore, calibrations of the current are taken for every experiment using ratios between the current measured through the Faraday cup and the sample holder. Typical ratios are from 0.75 to 0.9, depending on Li^+ energy. In addition, preliminary experiments of Li^+ on SS are taken to confirm f_{geo}.

However, this determination of the sputtering yield is precise only when materials on the QCM crystal are specified. Unfortunately, the sputtering yield of the lithiated graphite cannot be determined because the ratio of Li and C in sputtered materials is unknown. Therefore, the sputtered masses per incident ions before and after Li evaporation/D saturation are compared.

Uncertainty analysis is taken for every data point, and it ranges from 8% to 50%. Although many parameters for the ion source are strictly maintained during the experiment, these large errors came from an unstable Li^+ dose over the experiments since that Li^+ current is strongly affected by the temperature and the remaining amount of the solid LiCl source. A more detailed discussion of the determination of the sputtering yield by IIAX is discussed in [4].

III. Results and Discussion

A. System Calibration

To calibrate the system, a couple of experiments are run to measure the sputtering yields of SS by Li^+ and ATJ graphite by Ar^+. These results are shown in Fig. 4(a) and (b) with TRIM calculation results. These TRIM calculations were taken at the same geometry with the experiments at IIAX, where ions irradiate the surface at 45° incidence. Both results generally agree with the TRIM calculations. Although the sputtering yields of ATJ graphite by Ar^+ show higher yields than TRIM results, it could be explained by the remaining dust on the graphite surface, as discussed in the following section. Moreover, while the data point of the 2000-eV Ar^+ irradiation shows a smaller sputtering yield than predicted, it is explained by that reflected heavy Ar ions sputtered off the surface of the QCM crystal. Therefore, it is found that the Li ion beam and the ATJ graphite target are eligible in determining the sputtering yields. Hence, it is concluded that IIAX is a well-calibrated system in measuring the sputtering yield of graphite by Li^+ incidence.

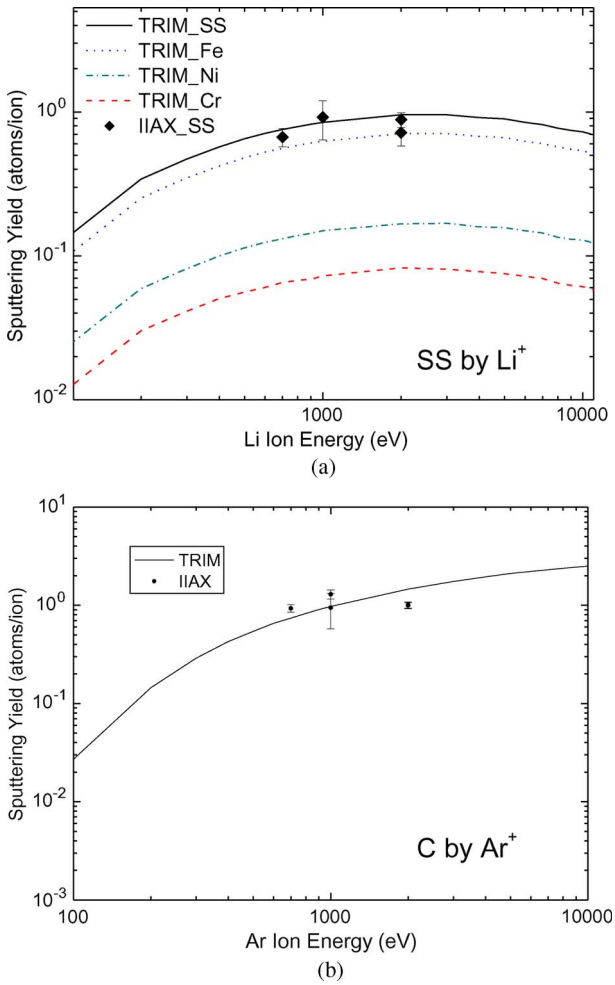

Fig. 4. Comparison of the experimental and computational sputtering yields of (a) lithium ions on SS and (b) argon ions on ATJ graphite at 45° incidence.

B. Sputtering of the ATJ Graphite by Li^+ Ions

Fig. 5 shows a comparison of the measured and calculated sputtering yields of ATJ graphite by Li^+. While dusty (circle) and He discharged (triangle) targets show large sputtering yields compared with the computational data, targets after scotch tape cleaning (square) show lower sputtering yields by a factor of two or more. He discharge cleaning was taken by using the same plasma cup used for D saturation, and a flux in the order of 10^{15} ions/(cm$^2 \cdot$ s) was obtained; however, it

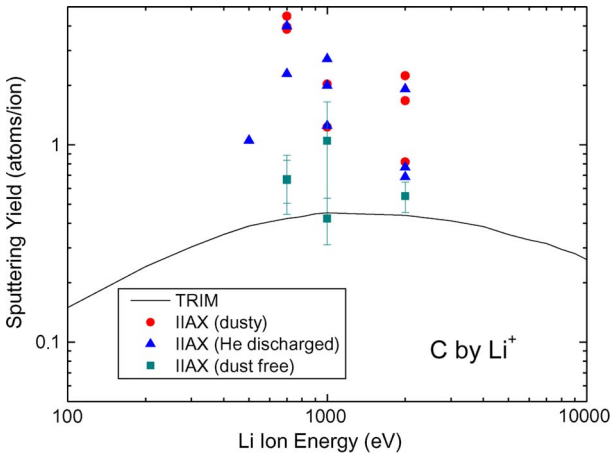

Fig. 5. Comparison of the experimental and computational sputtering yields of lithium ions on ATJ graphite at 45° incidence. Sputtering yields of (circle) dusty ATJ graphite, (triangle) after helium discharge cleaning, and (square) after scotch tape dust cleaning are shown.

is not an efficient way in completely eliminating large graphite particles. For the scotch tape cleaning, the sample surface is cleaned by the scotch tape until no sign of particles appears. There are higher sputtering yields for the sample before the scotch tape cleaning because the dust particles on the surface are easily released from the surface even with the kinetic energy lower than the surface binding energy. Although it is possible that this scotch tape cleaning contaminates the sample surface with its glue, it will not be a problem since the glue is also carbon or hydrocarbons. All other data shown in this paper are taken by using this dust-free ATJ graphite sample.

C. Sputtering of Li/ATJ Graphite and D-Li/ATJ Graphite by Li^+ Ions

Sputtered amounts from ATJ, Li/ATJ graphite, and D-Li/ATJ graphite samples are compared in Fig. 6. In this figure, the amount of sputtered particles from the surface per incident ion is plotted. Experimental data show lower sputtering amounts from Li^+ on lithiated ATJ graphite than Li^+ on ATJ graphite. In addition, compared with TRIM calculations, Li^+ on lithiated ATJ graphite shows even less sputtering amounts than Li self-sputtering. Furthermore, the TRIM calculations do not include the oxidation effect on the QCM crystal, while in the experiments, Li atoms on the QCM crystal do form lithium oxide. In particular, Li atoms can be preferentially sputtered compared with C atoms because of its lighter mass. Therefore, the actual experimental data points of the lithiated graphite could be lower than shown. This result shows the suppression of the sputtering yields for Li^+ on ATJ graphite after Li evaporation.

In addition, the Li^+ sputtering does the ion implantation of Li during measurement, but the sputtering yields of plain ATJ graphite do not change even for a long measurement (> 10 h). Therefore, this result indicates that Li implantation does not suppress sputtering, but Li evaporation does.

Although a previous study [4] shows a suppression of the sputtering yields of He^+ on solid lithium after D saturation, in our current study, the sputtered amounts from D-saturated lithiated graphite do not show significant difference from the

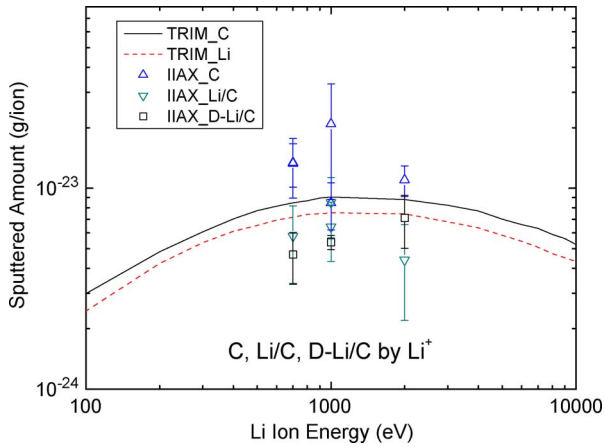

Fig. 6. Normalized sputtering amounts by a lithium ion on ATJ, lithiated ATJ, and D-saturated lithiated ATJ graphites at 45° incidence.

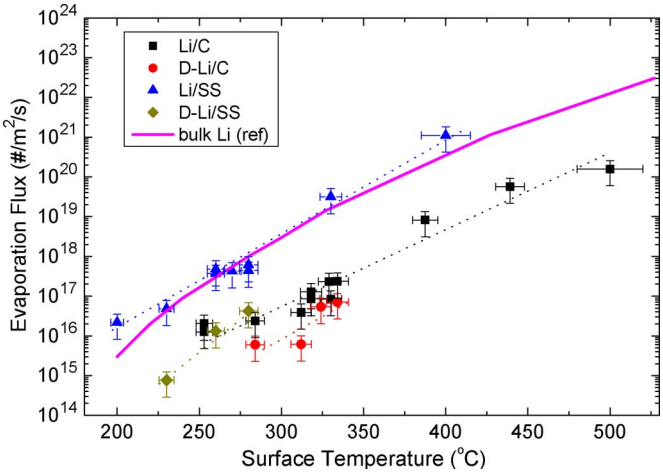

Fig. 7. Measured thermal evaporation fluxes of D-saturated and nonsaturated lithium on SS and lithiated ATJ graphite. Dotted lines are for the eyes.

nonsaturated sample. It could be because Li on graphite does not form Li-D bonds that could increase the surface binding energy, leading to smaller sputtering amounts. This is supported by a previous study [5] which indicates that lithium and hydrogen would be a neighbor, but they do not form Li-D bonds in graphite. Furthermore, it is also possibly contributing that Li^+ preferentially sputters Li than D because of mass differences.

D. Evaporation Flux

Fig. 7 shows the measured thermal evaporation fluxes of D-saturated and nonsaturated Li on SS and lithiated graphite. First, the measured evaporation flux of Li on SS agrees well with the known evaporation flux of bulk Li. This indicates that the measurement system is well calibrated and that the thin film of Li on SS can be regarded as bulk Li. The most important point of this figure is that the thermal evaporation flux from lithiated graphite shows a magnitudeless flux than Li on SS. The evaporation flux of the bulk Li at 400 °C, which is considered as a limit value for the lithium divertor operation, is equivalent to the evaporation flux of the intercalated Li in graphite at 500 °C. Therefore, the limit temperature could be set higher. This suppression might be explained by phase studies

of Li-intercalated graphite [6], [7]. According to these studies, the intercalated Li has a higher sublattice melting point in the graphite lattice, more than 220 °C if the concentration of Li is below 80% of the saturation, than the bulk Li whose melting point is around 180 °C. Although the exact value of concentration is uncertain, all samples in this paper should be below 80% since the evaporated lithium thickness was on the order of micrometer, while the sample thickness was on the order of millimeter.

In addition, a suppressed evaporation flux after D saturation is seen for Li on SS, while a little suppression is seen in the case of lithiated graphite. This can be explained again by the formation of the Li–D bonds. The Li–D formation possibly increases the melting point of Li, but such formation is unlikely in the case of lithiated graphite. Therefore, D saturation suppresses the evaporation of Li on SS but not for the lithiated graphite.

IV. Conclusion

Absolute sputtering yields of Li^+ on ATJ graphite and lithiated ATJ graphite before and after D saturation at 45° incidence are measured. Suppressed sputtering yields are detected after the Li evaporation treatment of the ATJ graphite. This result indicates that lithium atoms preferentially sputter Li instead of graphite. Also, D saturation did not change the sputtering results, which can be explained by the preferential sputtering of Li atoms by Li^+ and the unlikely formation of Li-D bonds in the graphite. In addition, the evaporation flux of Li and lithiated ATJ graphite is measured. The suppressed evaporation flux of the intercalated Li in graphite is observed for surface temperatures ranging from 250 °C to 500 °C.

References

[1] H. W. Kugel, M. G. Bell, J.-W. Ahn, J. P. Allain, R. Bell, J. Boedo, C. Bush, D. Gates, T. Gray, S. Kaye, R. Kaita, B. LeBlanc, R. Maingi, R. Majeski, D. Mansfield, J. Menard, D. Mueller, M. Ono, S. Paul, R. Raman, A. L. Roquemore, P. W. Ross, S. Sabbagh, H. Schneider, C. H. Skinner, V. Soukhanovskii, T. Stevenson, J. Timberlake, W. R. Wampler, and L. Zakharov, "The effect of lithium surface coatings on plasma performance in the National Spherical Torus Experiment," *Phys. Plasmas*, vol. 15, no. 5, pp. 056 118–056 118-13, May 2008.

[2] N. Itou, H. Toyoda, K. Morita, and H. Sugai, "Rapid diffusion of lithium into bulk graphite in lithium conditioning," *J. Nucl. Mater.*, vol. 290–293, pp. 281–285, Mar. 2001.

[3] J. N. Brooks, "Modeling of sputtering erosion/redeposition—Status and implications for fusion design," *Fusion Eng. Des.*, vol. 60, no. 4, pp. 515–526, Jul. 2002.

[4] J. P. Allain and D. N. Ruzic, "Measurements and modelling of solid phase lithium sputtering," *Nucl. Fusion*, vol. 42, no. 2, pp. 202–210, Feb. 2002.

[5] J. R. Dahn, T. Zheng, Y. Liu, and J. S. Xue, "Mechanisms for lithium insertion in carbonaceous materials," *Science*, vol. 270, no. 5236, pp. 590–593, Oct. 1995.

[6] K. C. Woo, H. Mertwoy, J. E. Fischer, W. A. Kamitakahara, and D. S. Robinson, "Experimental phase diagram of lithium-intercalated graphite," *Phys. Rev. B, Condens. Matter*, vol. 27, no. 12, pp. 7831–7834, Jun. 1983.

[7] D. P. DiVincenzo and T. C. Koch, "Theoretical phase diagram for Li-intercalated graphite," *Phys. Rev. B, Condens. Matter*, vol. 30, no. 12, pp. 7092–7096, Dec. 1984.

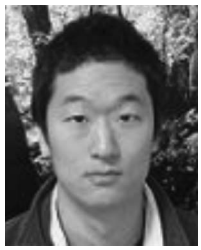

Kenzo Ibano (M'09) was born in Evanston, IL, in 1985. He received the B.S. degree in applied physics from Keio University, Yokohama, Japan, in 2007. He is currently working toward the M.S. degree in the Department of Nuclear, Plasma, and Radiological Engineering, University of Illinois at Urbana-Champaign, Urbana.

Vijay Surla was born in Visakhapatnam, India, in 1980. He received the Ph.D. degree in mechanical engineering from Colorado State University, Fort Collins, in 2007.

He is currently with the Center for Plasma Material Interactions, University of Illinois at Urbana–Champaign, Urbana. His research interests include diagnostic techniques in plasma material interactions, with applications in electric propulsion, fusion energy, and extreme ultraviolet lithography.

David N. Ruzic (M'01) received the Ph.D. degree in physics from Princeton University, Princeton, NJ, in 1984.

He is currently a Professor with the Department of Nuclear, Plasma, and Radiological Engineering, University of Illinois at Urbana–Champaign, Urbana. He joined the faculty in 1984 after receiving the Ph.D. degree and doing postdoctoral work at the Princeton Plasma Physics Laboratory. His research centers on the interaction of plasmas with materials; applications include magnetic fusion energy, as well as microelectronic processing. He has a passion for teaching, particularly about energy sources, because he gets to blow something up in almost every class.